Talanta 134 (2015) 482–487

Contents lists available at ScienceDirect

Talanta

journal homepage: www.elsevier.com/locate/talanta

Rhodium nanoparticle-modified screen-printed graphite electrodes for the determination of hydrogen peroxide in tea extracts in the presence of oxygen

Vasiliki A. Gatselou, Dimothenis L. Giokas, Athanasios G. Vlessidis, Mamas I. Prodromidis *

Department of Chemistry, University of Ioannina, Ioannina 45110, Greece

ARTICLE INFO

Article history:
Received 12 September 2014
Received in revised form
7 November 2014
Accepted 17 November 2014
Available online 25 November 2014

Keywords:
Hydrogen peroxide
Tea
Antioxidant activity
Rhodium nanoparticle
Screen-printed graphite electrodes
Chemical sensors

ABSTRACT

In this work we describe the fabrication of nanostructured electrocatalytic surfaces based on polyethyleneimine (PEI)-supported rhodium nanoparticles (Rh-NP) over graphite screen-printed electrodes (SPEs) for the determination of hydrogen peroxide in the presence of oxygen. Rh-NP, electrostatically stabilized by citrate anions, were immobilized over graphite SPEs, through coulombic attraction on a thin film of positively charged PEI. The functionalized sensors, polarized at 0.0 V vs. Ag/AgCl/3 M KCl, exhibited a linear response to H_2O_2 over the concentration range from 5 to 600 μmol L^{-1} H_2O_2 in the presence of oxygen. The 3σ limit of detection was 2 μmol L^{-1} H_2O_2, while the reproducibility of the method at the concentration level of 10 μmol L^{-1} H_2O_2 ($n=10$) and between different sensors ($n=4$) was lower than 3 and 5%, respectively. Most importantly, the sensors showed an excellent working and storage stability at ambient conditions and they were successfully applied to the determination of H_2O_2 produced by autooxidation of polylphenols in tea extracts with ageing. Recovery rates ranged between 97 and 104% suggesting that the as-prepared electrodes can be used for the development of small-scale, low-cost chemical sensors for use in on-site applications.

1. Introduction

The inherent advantages associated with the electrochemical detection of hydrogen peroxide (e.g. high sensitivity and selectivity, rapid response, low cost, simple instrumentation and easy miniaturization) have pushed methods based on electrochemical sensors and biosensors at the forefront of scientific research. Although a plentiful of electrochemical sensors based on Prussian blue [1,2] and other electrocatalysts [3–5], conducting polymers [6,7] and enzyme-based biosensors [3,8–10] have been developed, the drive over the last years is tipped in favor of metal nanoparticles (NP)-based sensors [11–13]. Such sensors offer unique advantages in terms of sensitivity, selectivity, compatibility with living organisms and working stability. Moreover, due to their ultra-fine dimensions and high electroactive surface area they provide unique opportunities for incorporation in miniaturized and low-cost substrates, thus giving rise to the provision of expedient solutions to the most contemporary demands in chemical sensing such as, on-site applications, in-vivo monitoring, tissue-embedded flexible sensor-based alarm systems etc [14,15].

A big obstacle to the use of metal NP-based hydrogen peroxide sensors is their inherent electrocatalytic activity to the reduction of dissolved oxygen, which restricts their use only in deaerated solutions. Beyond practical difficulties associated with sample deaeration outside the laboratory, deoxygenation of the sample may also affect the analysis due to volatility of H_2O_2 [16]. To date, the only NP-based electrochemical sensors that have been reported to enable the selective reduction of hydrogen peroxide in the presence of oxygen rely on phosphonate functionalized Pt nanoclusters [17] but they exhibit mediocre stability over time (~1 month) and their analytical utility has only been verified in standard solutions.

Among the vast gamut of nanoparticle-based electrochemical sensors, rhodium nanoparticles (Rh-NP) are the least represented. The only efforts made to exploit the potential utility of nanometer sized Rh particles in analytical applications focus on hybrid materials such as dendrimer-Rh-NP [18] and porous Rh nanotubes [19] for the detection of H_2O_2, Rh-NP-loaded carbon nanofibers for the determination of hydrazine [20] and Rh-NP–carbon nanospheres for H_2 sensing [21]. Beyond the demanding synthetic efforts, all these sensors are still at an early stage of development and as such their use in real samples has not been evaluated. Additionally, oxygen removal from all solutions is necessary to alleviate its interference, which limits their application to on-site

* Corresponding author. Tel.: +30 26510 08301; fax: +30 26510 08796.
E-mail address: mprodrom@cc.uoi.gr (M.I. Prodromidis).

http://dx.doi.org/10.1016/j.talanta.2014.11.033
0039-9140/

analysis. Therefore, there is a large gap regarding the realistic use of Rh-NP as electrochemical sensors.

In this work, we present for the first time an electrochemical sensor based on Rh-NP nanoparticles for the determination of H_2O_2 in complex samples in the presence of dissolved oxygen. The sensors were modified by a simple drop-casting deposition of Rh-NP on the surface of graphite screen printed electrodes. Immobilization was accomplished by electrostatic attraction between the negative surface charge of Rh-NP and positively charged polyethyleneimine (PEI) previously functionalized on the surface of the electrodes. A remarkable electrocatalytic response for the reduction of hydrogen peroxide was recorded, even in the presence of oxygen, thus alleviating the need for sample deaeration. The newly devised sensor was applied to monitor the H_2O_2-generating ability of aqueous tea extracts, which is produced by autooxidation of polylphenols and may negatively affect living systems due to its pro-oxidant action [22]. The facile fabrication procedure along with the improved analytical performance in terms of selectivity, sensitivity and the exceptional working stability of the sensor under realistic conditions, suggest that Rh-NP hold great promise to the fabrication of low cost, disposable sensors for in-field detection of H_2O_2.

2. Experimental

2.1. Materials

Citric acid, polyethyleneimine (PEI, brunched, M.W. ~2000 by LS), and sodium borohydride were purchased from Sigma-Aldrich. Catalase from bovine liver (M.W. ~240,000, ≥200,000 U mL^{-1}) and $RhCl_3 \times 3H_2O$ (38% in Rh) were obtained from Fluka and Merck, respectively. All other reagents were of analytical grade and were used without further purification. Double distilled water (DDW) was used throughout. A stock solution of approximately 0.1 mol L^{-1} H_2O_2 was prepared by appropriate dilution of the concentrated solution (>30% H_2O_2, Fluka) in DDW, stored at +4 °C and was weekly standardized with the $KMnO_4$ titrimetric method.

2.2. Preparation of rhodium colloidal suspension

Rhodium nanoparticles were prepared according to an earlier work [23] by reducing 0.765 mmol L^{-1} of $RhCl_3 \times 3H_2O$ with 5 mmol L^{-1} $NaBH_4$ in the presence of 0.5 mmol L^{-1} citrate ions, which were used as morphology regulators and stabilizers. After 15 min of mixing the color of the suspension turned to dark brown–green. Based on dynamic light scattering data, the average hydrodynamic diameter of the rhodium nanoparticles was found to be 8.7 nm (Fig. S1, Supporting information).

2.3. Fabrication of screen-printed electrodes

Low-cost, all-graphite screen-printed electrodes (SPEs) were fabricated over a 125 μm thick flexible polyester substrate (Mac Dermid) using a DEK 247 screen printer and polyester screens (280 mesh, DEK). Graphite ink (PF-407A, Acheson) was forced through a 13–20 μm thick emulsion with the desired pattern using a polyurethane 75 durometer squeegee. Before measurements, the conductive track was covered with an insulating tape (RS components). Details on the fabrication process are given in a previously published work [24].

2.4. Instrumentation

Cyclic voltammetry (CV), amperometry and electrochemical impedance spectroscopy (EIS) experiments were performed with the electrochemical analyzer Autolab PGSTAT12/FRA2 in a one-compartment three-electrode cell. Bare or modified SPEs and a platinum wire were served as the working and auxiliary electrodes, respectively. The reference electrode was a Ag/AgCl/3 M KCl (IJ Cambria) electrode and all potentials reported hereafter refer to the potential of this electrode. CV and amperometry experiments were performed in a solution of 0.1 mol L^{-1} phosphate buffer solution containing 0.1 mol L^{-1} KCl (PBS), pH 7, at room temperature, using a scan rate of 0.1 V s^{-1} and at a polarization potential 0.0 V (unless stated otherwise), respectively. The impedance spectra were recorded over the frequency range 10^{-1}–10^5 Hz, using a sinusoidal excitation signal, superimposed on a DC potential of 0.200 V. Excitation amplitude of 10 mV (rms) was used throughout. EIS measurements were performed in a solution 0.1 mol L^{-1} PBS, pH 7, at room temperature, in the presence of 5 mmol L^{-1} hexacyanoferrate (II)/(III) (1+1 mixture), which used as redox probe.

Scanning electron images and elemental microprobe analysis were performed on a JEOL JSM-6510LV scanning electron microscope equipped with an INCA PentaFETx3 (Oxford Instruments) energy dispersive X-ray (EDX) spectroscopy detector. Data acquisition was performed with an accelerating voltage of 20 kV and 60 s accumulation time. Samples were coated with a 15-nm-thick film of Au using a Polaron SC7620 sputtercoater by Thermo VG Scientific.

2.5. Preparation of the tea extracts

Tea samples (black and green) were purchased from the local market. An amount of 3.00 g of each sample was added in 50.00 mL 0.1 mol L^{-1} PBS pH 7, and the mixture was heated at 90 °C for 30 min under stirring. The mixture left to cool at room temperature, centrifuged at 5000 rpm for 30 min and then filtered through a Millipore membrane (0.45 μm pore size). For the recovery studies, the sample was fortified with 1.43 mmol L^{-1} H_2O_2. Control samples were prepared in a similar manner by also adding 10 μL catalase.

2.6. Analytical procedure

A (65.00 − x)-mL aliquot of PBS was introduced in the reaction cell and stirred at a moderate speed with a magnetic stirrer. When a stable current value was reached, appropriate amounts (xmL) of H_2O_2 or tea extract samples were added, and current changes due to the electro reduction of H_2O_2 at 0.0 V were recorded. The steady-state current response was taken as a measure of the analyte concentration.

Calibration curves at different working ranges were constructed by adding 5 (2 first additions), 10 (next 18 additions) and 100 (next 9 additions) μmol L^{-1} H_2O_2 in the measuring cell.

3. Result and discussion

3.1. Electrochemical behaviour of SPEs/Rh-NP

The CV plots of bare and Rh-NP-modified SPEs in 0.5 mol L^{-1} H_2SO_4 deaerated solution are illustrated in Fig. 1. The pattern of the recoded CV can be explained as follows: In the hydrogen region, the sharp increase of the current at potential values more cathodic than −0.100 V can be collectively attributed to the adsorption of hydrogen ions and to the hydrogen evolution

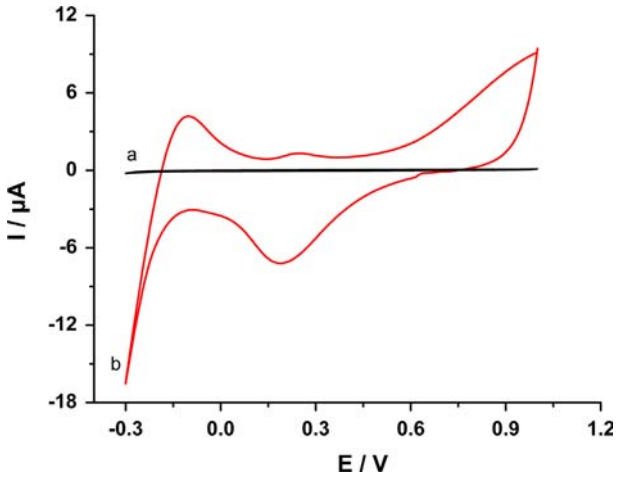

Fig. 1. CVs of bare (scan a) and Rh-NP-modified SPEs (scan b) in 0.5 mol L^{-1} H_2SO_4 solution deaerated with high purity N_2. Scan rate 0.1 V s^{-1}.

process while the peak that appeared at −0.125 V during the anodic scan is associated with the oxidation of the absorbed hydrogen [25]. At more positive potential values, during the anodic scan, the peak at 0.270 V can be ascribed to the charging of the double layer due to the adsorption of hydrogen sulphate ions [25,26], while the onset of the formation of Rh surface oxide appeared at 0.500 V. Finally, the large peak at 0.180 V during the cathodic scan corresponds to the reduction of the oxide layer.

3.2. Electrocatalysis and buildup of the sensors

As can be seen from the CVs illustrated in Fig. 2A, Rh-NP endowed graphite SPEs with enhanced electrocatalytic properties towards both the oxidation and reduction of hydrogen peroxide. Whereas bare SPEs produced no catalytic currents upon the addition of hydrogen peroxide (scans a, a′), Rh-NP deposited onto SPEs either through physical absorption (scans b, b′) or through electrostatic forces (scans c, c′) onto PEI-modified SPEs, gave rise to large catalytic currents. By comparing the magnitude of the catalytic currents at SPEs/Rh-NP (scans b, b′) and SPEs/PEI/Rh-NP (scans c, c′) it is evident that the presence of a thin film of PEI onto the surface of the graphite SPEs acts beneficially on the electrocatalytic performance of the sensor. The effect of PEI at five discrete concentrations (0.1, 0.2, 0.5, 1.0 and 2.0% w/v in ethanol) was investigated by performing comparative CV catalytic experiments in the presence of 5 mmol L^{-1} H_2O_2. The highest catalytic currents were observed at SPEs/PEI(0.2%)/Rh-NP. Slightly lower catalytic currents were observed at SPEs/PEI(0.1%)/Rh-NP, while at higher concentrations of PEI (0.5–2.0% w/v in ethanol) no improvement in the catalytic performance was observed. In all occasions, the catalytic currents were higher than those obtained by SPEs/Rh-NP. Comparative chronoamperometric plots for three selected sensors modified with 0, 0.2 and 2.0% w/v PEI in ethanol are illustrated in Fig. 2B.

The formation of each layer was investigated by performing faradic EIS during the various modification steps. As can been seen in the Bode plots illustrated in Fig. 3, at the low frequency range, which describes the impedimetric behavior of the electrode/electrolyte interface, the bare graphite SPEs (scan a, filled circles) exhibit an increased impedance value ($\log|Z| = 3.47\ \Omega$ at 0.1 Hz) that dramatically reduced ($\log|Z| = 3.02\ \Omega$ at 0.1 Hz) at SPEs/PEI (0.2%) (scan b, filled squares). This drastic drop of the interfacial impedance is attributed to an increased flux of the redox probe to the surface of the electrode due to the electrostatic attraction of the negatively charged hexacyanoferrate (II)/(III) molecules by the positively-charged amino ($-NH_3^+$) groups in PEI film. Further decrease of the interfacial impedance ($\log|Z| = 2.96\ \Omega$ at 0.1 Hz) at SPEs/PEI(0.2%)/Rh-NP (scan c, filled diamonds) can be collectively attributed to the enhancement of the electrocatalytic performance

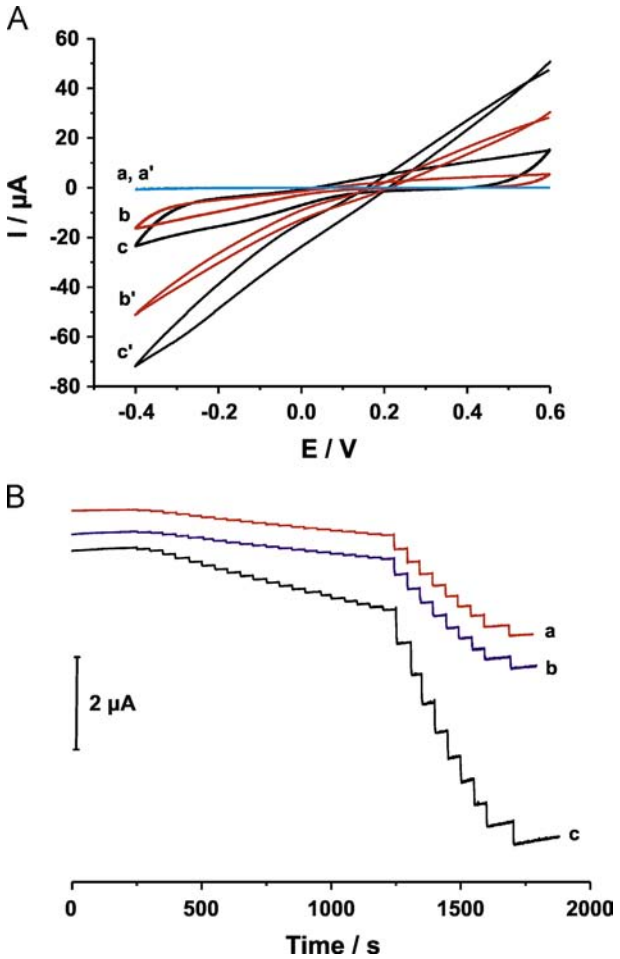

Fig. 2. (A) CVs of (a and a′) bare SPEs, (b and b′) SPEs/Rh-NP and (c and c′) SPEs/PEI (0.2%)/Rh-NP in 0.1 mol L^{-1} PBS pH 7 containing 0.1 mol L^{-1} KCl (a–c) before and (a′, b′, c′) after the addition of 5 mmol L^{-1} H_2O_2; Scan rate 0.1 V s^{-1}. (B) Chronoamperometric plots of SPEs/PEI/Rh-NP sensors modified with (a) 0, (b) 2 and (c) 0.2% w/v PEI in ethanol over the concentration range 5–1090 μmol L^{-1} H_2O_2 at 0.0 V in 0.1 mol L^{-1} PBS pH 7 containing 0.1 mol L^{-1} KCl in the presence of dissolved oxygen.

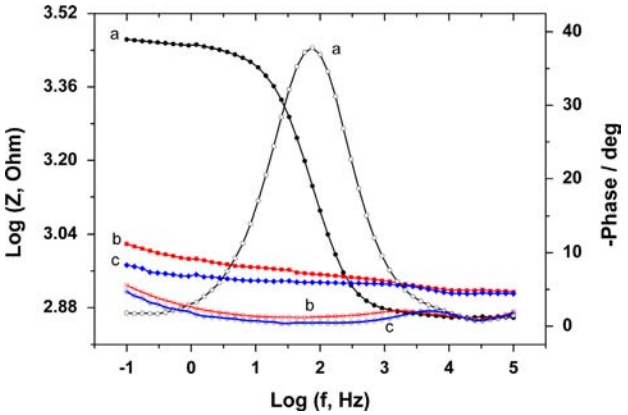

Fig. 3. Bode plots of the sensors at various modification steps: (scan a, circles) bare SPE, (scan b, squares) SPEs/PEI(0.2%), and (scan c, diamonds) SPEs/PEI(0.2%)/Rh-NP in 0.1 mol L^{-1} PBS pH 7 containing 5 mmol L^{-1} hexacyanoferrate (II)/(III). Filled symbols, impedance profile; empty symbols, phase profile.

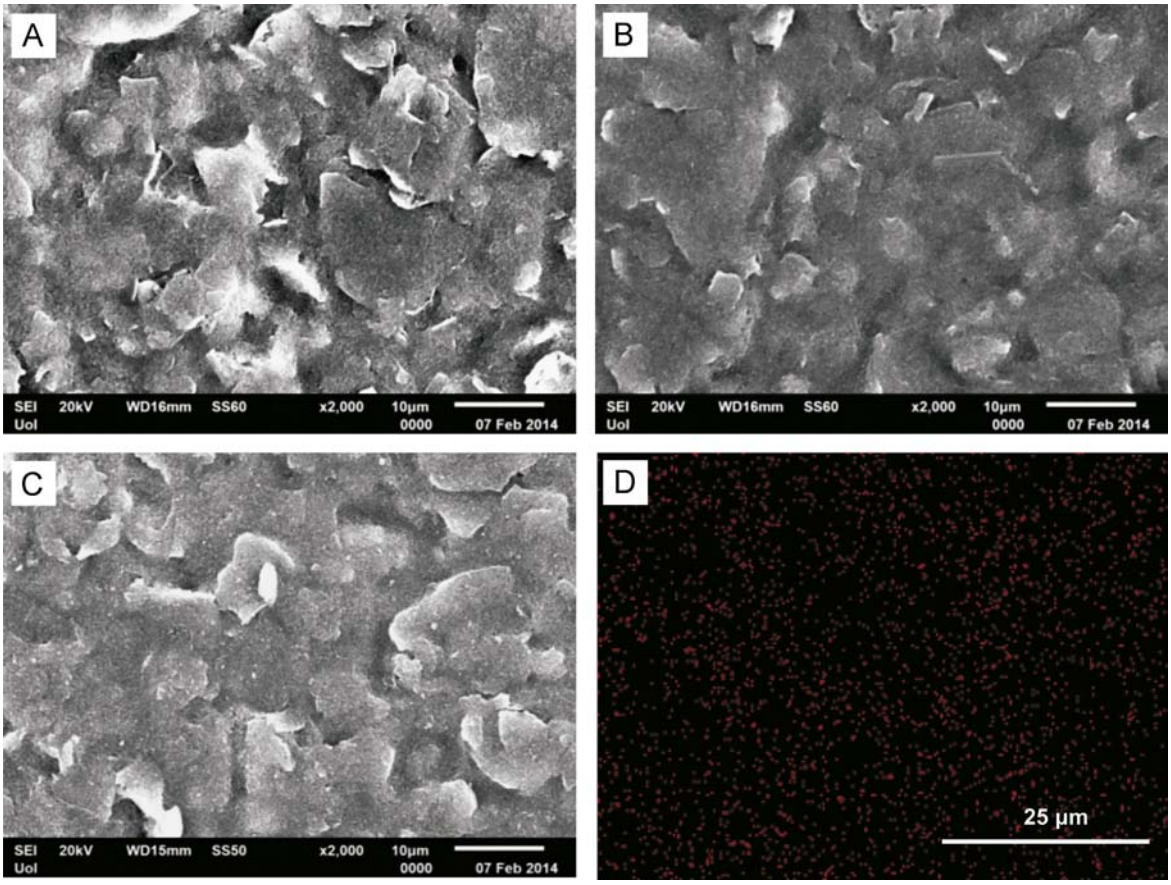

Fig. 4. SEM images of (A) bare SPEs, (B) SPEs/PEI(0.2%) and (C) SPEs/PEI(0.2%)/Rh-NP assemblies. (D) EDX elemental map microanalysis of (C).

of the electrode surface and to the lowering of the resistance of PEI/Rh-NP film due to the presence of the metal nanoparticles. Over the high frequency range, the observed difference of impedance values between the bare and the two modified SPEs can be attributed to alterations of the ohmic resistance of the active surface due to exposure to ethanol during the deposition of the PEI film [27]. In all three cases, the empty symbols plots show the corresponding phase profiles.

From the SEM images illustrated in Fig. 4 it can be inferred that the development of the PEI film over the screen-printed graphite layer smoothes out its morphological characteristics (Fig. 4B and C) preventing the inclusion, and the subsequent agglomeration of Rh-NP into the cavities. On the other hand, grooves appear at the heterogeneous surface of bare SPEs (Fig. 4A). The lower surface roughness at SPEs/PEI sensors along with the interaction induced by the positively charged amino groups at the film of PEI facilitate Rh-NP to be uniformly distributed over the surface of the electrodes as evidenced by elemental EDX mapping (Rh atoms are colored in red) acquired across representative areas of the sample (Fig. 4D and Fig. S2).

3.3. Optimization of experimental variables

The effect of dissolved oxygen on the electrocatalytic performance of SPEs/PEI(0.2%)/Rh-NP was initially evaluated by performing comparative CV studies in non-deaerated (b, b′) and deaerated (a, a′) solution of PBS, before and after the addition of H_2O_2 (Fig. 5). By comparing scans (a, b) it can be inferred that Rh-NP exhibit a rather moderate electrocatalysis towards dissolved oxygen as revealed by the magnitude of the cathodic catalytic wave at scan (b), which disappeared at scan (a) in the N_2-saturated electrolyte. The competitive role of dissolved oxygen to the electro reduction of H_2O_2 can be seen by comparing the magnitude of the catalytic waves [scans (a′), (b′)] recorded after the addition of 5 mmol L^{-1} H_2O_2. A detailed appraisal of the interfering effect of dissolved oxygen on the electro reduction of H_2O_2 at SPEs/PEI (0.2%)/Rh-NP was made by performing a series of chronoamperometric measurements at different polarization potential values. The catalytic currents recorded at 0.050, 0.0, −0.050, −0.100, −0.200 and −0.300 V verify the ability of SPEs/PEI(0.2%)/Rh-NP sensors to measure H_2O_2 at the micromolar range in the presence of dissolved oxygen at polarization potential values less cathodic than −0.200 V, where the interference effect of dissolved oxygen becomes significant. Taking as criteria the observed sensitivity, the magnitude of the background current and the time required to reach a stable baseline, further experiments were performed at 0.0 V. It is noted however, that polarization potential values of −0.050 and −0.100 V also provide excellent *I*–*t* curves and can alternatively be used for applications in samples rich in reducing compounds.

The pH of the working buffer was also investigated by recording the signal changes of SPEs/PEI(0.2%)/Rh-NP in the presence of 50 μmol L^{-1} H_2O_2. Experiments were conducted in 0.1 mol L^{-1} PBS covering the pH range 5–8 and the results showed that the sensors exhibit excellent performance over the pH range 6–8, while the highest response was observed at pH 7, which was therefore used for the subsequent work.

The optimum volume of the Rh colloidal solution deposited onto the electrodes was also investigated by applying 2, 5, 10, 15 and 20 μL of Rh-NP suspension onto the surface of the PEI-modified SPEs. The sensitivity of the resulting sensors increased with increasing volumes up to 15 μL, slightly leveling off thereafter. Therefore, the application of 15 μL of RhNP solution was selected as optimum.

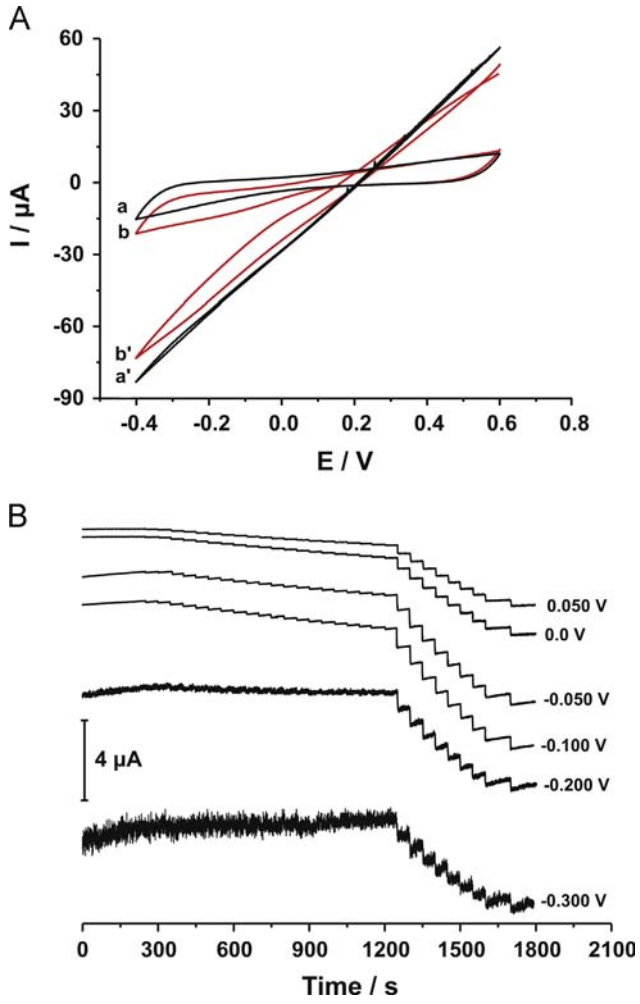

Fig. 5. (A) CVs of SPEs/PEI(0.2%)/Rh-NP in (a and a′) deaerated and (b and b′) non-deaerated solution of 0.1 mol L^{-1} PBS pH 7 containing 0.1 mol L^{-1} KCl, (a and b) before and (a′ and b′) after the addition of 5 mmol L^{-1} H_2O_2; Scan rate, 0.1 V s^{-1}. (B) Chronoamperometric plots of SPEs/PEI(0.2%)/Rh-NP over the concentration range 5–1090 μmol L^{-1} H_2O_2 at (a) 0.050, (b) 0.0, (c) −0.050, (d) −0.100, (e) −0.200 and (f) −0.300 V in 0.1 mol L^{-1} PBS pH 7 containing 0.1 mol L^{-1} KCl in the presence of dissolved oxygen.

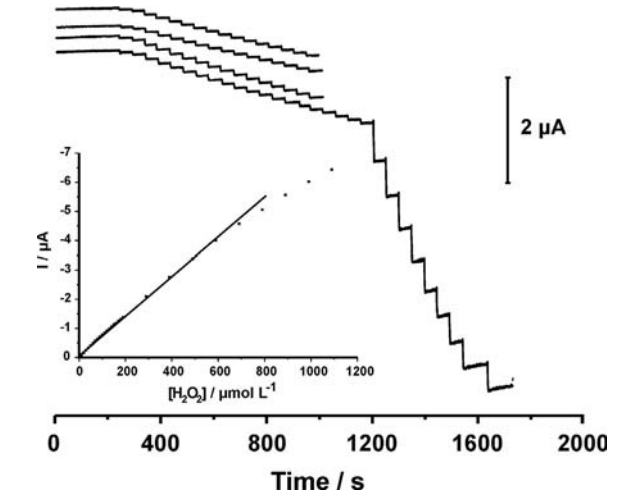

Fig. 6. Chronoamperometric plots of different SPEs/PEI(0.2%)/Rh-NP over the concentration range 5–150 μmol L^{-1} (5–1090 μmol L^{-1} for the electrode used for the construction of inset calibration curve) H_2O_2 at 0.0 V in 0.1 mol L^{-1} PBS pH 7 containing 0.1 mol L^{-1} KCl in the presence of dissolved oxygen. The inset graph illustrates the corresponding I=f [H_2O_2] plot.

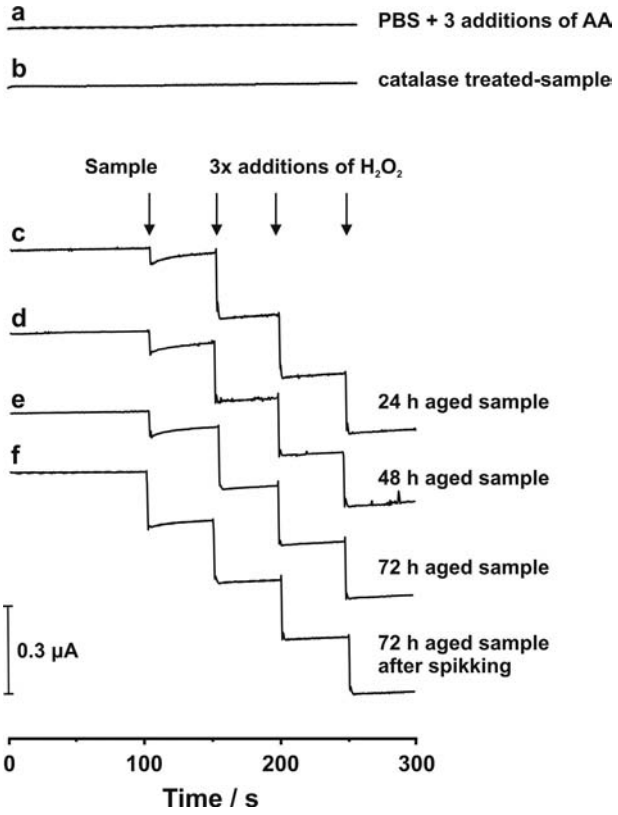

Fig. 7. Chronoamerometric plots for the determination of H_2O_2 in the green tea extract, sample 1. Plots a and b show the response of the sensor after three successive additions of 25 μmol L^{-1} ascorbic acid in the solution of pure electrolyte, and to the catalase-treated sample, respectively. Standard addition method (sample+3 sequential additions of 50 μmol L^{-1} H_2O_2) after an ageing period of (plot c) 24 h, (plot d) 48 h and (plot e) 72 h. Plot f refers to the 72 h-aged sample after spiking with 22.0 μmol L^{-1} H_2O_2. Measurements were conducted at 0.0 V in 0.1 mol L^{-1} PBS pH 7 containing 0.1 mol L^{-1} KCl in the presence of dissolved oxygen. (For interpretation of the references to color in this figure legend, the reader is referred to the web version of this article.)

3.4. Analytical performance

Under the optimum experimental conditions the dependence of the electrocatalytic currents on different concentrations of hydrogen peroxide was recorded (Fig. 6). The plot of I(current/μA)=f([H_2O_2/μmol L^{-1}]) was rectilinear over the range 5–600 μmol L^{-1} H_2O_2 with a coefficient of determination, R^2=0.9982 (Fig. 6, inset graph). The detection limit, for a signal-to-noise ratio of 3, was 2 μmol L^{-1} H_2O_2 while the relative standard deviation (RSD) of the method was less than 3% (n=10, 10 μmol L^{-1} H_2O_2). The reproducibility between different sensors was also assessed by comparing the responses of four different sensors over the concentration range 5–150 μmol L^{-1} H_2O_2. The comparison of the received chronoamperometric plots illustrated in Fig. 6 justifies the excellent reproducibility of the sensors, which can be further improved by automating the procedure for the application of the supporting and sensing films.

Finally, the sensors displayed excellent storage stability when stored dry at ambient conditions retaining more than 95% of their initial activity for a least four months.

3.5. Application to real samples

The developed sensors were applied to the determination of hydrogen peroxide in tea extracts. The selectivity of the sensors was initially investigated by three successive additions of 25 μmol L^{-1} ascorbic acid, a potent electroactive compound, in the pure electrolyte solution (Fig. 7, plot a), and by the addition of

Table 1
Determination and recovery studies of H_2O_2 in various tea extracts after a 65-fold dilution in 0.1 mol L^{-1} PBS, pH 7 containing 0.1 mol L^{-1} KCl. Concentrations are in μmol L^{-1} and are referring to the concentration of H_2O_2 in the measuring cell.

Sample	[H_2O_2] after the ageing of the samples for			Added, [H_2O_2]	Found, [H_2O_2]	Recovery %
	24 h	48 h	72 h			
Green tea, sample #1	15.0	26.7	35.0	22.0	55.6	97.5
Green tea, sample #2	13.9	23.3	23.8	22.0	47.5	103.7
Black tea	44.4	69.0	66.2	22.0	86.8	98.4

1.0 mL of the catalase-treated samples in the measuring cell (Fig. 7, plot b). In both occasions, zero or almost zero signal was recorded indicating that the sensors are highly selective for hydrogen peroxide.

The H_2O_2-generating ability of green and black tea extracts, arising from polyphenols oxidation, was then investigated by ageing the samples for 24, 48 and 72 h using the standard addition method (Fig. 7, plots c, d, e). Each sample was analyzed after a 65-fold dilution in order to mitigate the potential interfering effect of the various reducing compounds present in the samples. The results are summarized in Table 1. Finally, the accuracy of the method was verified by recovery experiments performed by fortifying the 72 h aged samples with 22 μmol L^{-1} H_2O_2 (Fig. 7, plot f). Recoveries were lying between 97 and 104% (Table 1), and justify the validity of the developed sensors for the determination of hydrogen peroxide in real samples in the presence of oxygen.

4. Conclusions

This work employs functional sensors based on polyethyleneimine-supported rhodium nanoparticles over graphite screen-printed electrodes for the determination of hydrogen peroxide in the presence of oxygen. Compared with other rhodium nanoparticle-modified electrodes, the fabricated electrodes show superior analytical performance in terms of sensitivity, storage and working stability. Moreover, they represent the first example of rhodium nanoparticle-based sensors that used for the determination of hydrogen peroxide in real samples. The successful application of the sensors to real samples along with their facile preparation over disposable, low-cost screen-printed graphite electrodes verifies their suitability in routine analysis. Their use in the presence of dissolved oxygen holds promise for in-field analysis of H_2O_2 in portable electroanalytical devices.

Appendix A. Supporting information

Supplementary data associated with this article can be found in the online version at http://dx.doi.org/10.1016/j.talanta.2014.11.033.

References

[1] F. Ricci, G. Palleschi, Biosens. Bioelectron. 21 (2005) 389–407.
[2] A.A. Karyakin, Electroanalysis 13 (2001) 813–819.
[3] L. Giannoudi, E.V. Piletska, S.A., Piletsky, Development of Biosensors for the Detection of Hydrogen Peroxide in Biotechnological Applications of Photosynthetic Proteins: Biochips, Biosensors and Biodevices, Eds. M.T. Giardi, E.V. Piletska, Landes Bioscience 2006, chapter 16.
[4] N. Sun, L. Guan, Z. Shi, N. Li, Z. Gu, Z. Zhu, M. Li, Y. Shao, Anal. Chem. 78 (2006) 6050–6057.
[5] T. Wang, H. Zhu, J. Zhuo, Z. Zhu, P. Papakonstantinou, G. Lubarsky, J. Lin, M. Li, Anal. Chem. 85 (2013) 10289–10295.
[6] D. Raffa, K.T. Leung, F. Battaglini, Anal. Chem. 75 (2003) 4983–4987.
[7] G. Li, Y. Wang, H. Xu, Sensors 7 (2007) 239–250.
[8] H. Song, Y. Ni, S. Kokot, Anal. Chim. Acta 788 (2013) 24–31.
[9] S. Ahammad AJ, J. Biosens. Bioelectron. (2013), http://dx.doi.org/10.4172/2155-6210.S9-001.
[10] W. Chen, S. Cai, Q.-Q. Ren, W. Wen, Y.-D. Zhao, Analyst 137 (2012) 49–58.
[11] J.M. Pingarron, P. Yanez-Sedeno, A. Gonzalez-Cortes, Electrochim. Acta 53 (2008) 5848–5866.
[12] W. Siangproh, W. Dungchai, P. Rattanarat, O. Chailapakul, Anal. Chim. Acta 690 (2011) 10–25.
[13] S. Chen, R. Yuan, Y. Chai, F. Hu, Microchim. Acta 180 (2013) 5–32.
[14] D. Kuhlmeier, N. Sandetskaya, S. Allelein, Recent Patents Food Nutr. Agric. 4 (2012) 187–199.
[15] G. Doria, J. Conde, B. Veigas, L. Giestas, C. Almeida, M. Assuncao, J. Rosa, P.V. Baptista, Sensors 12 (2012) 1657–1687.
[16] Y. Gu, C.-C. Chen, Sensors 8 (2008) 8237–8247.
[17] J. Xu, X. Wu, G. Fu, X. Liu, Y. Chen, Y. Zhou, Y. Tang, T. Lu, Electrochim. Acta 80 (2012) 233–239.
[18] S. Chandra, K.S. Lokesh, A. Nicolai, H. Lang, Anal. Chim. Acta 632 (2009) 63–68.
[19] F. Muench, C. Neetzel, S. Kaserer, J. Brötz, J.-C. Jaud, Z.Z. Karger, S. Lauterbach, H.-J. Kleebe, C. Rothac, W. Ensinger, Mater. Chem. 22 (2012) 12784–12791.
[20] G. Hu, Z. Zhou, Y. Guo, H. Hou, S. Shao, Electrochem. Commun. 12 (2010) 422–426.
[21] B.R. Sathe, RSC Adv. 3 (2013) 5361–5365.
[22] M. Akagawa, T. Shigemitsu, K. Suyama, Biosci. Biotechnol. Biochem. 67 (2003) 2632–2640.
[23] C. Jin, W. Xia, T.C. Nagaiah, J. Guo, X. Chen, N. Li, M. Bron, W. Schuhmann, M. Muhler, Chem. Mater. 20 (2010) 736–742.
[24] N. Lezi, C. Kokkinos, A. Economou, M.I. Prodromidis, Sens. Actuators B 182 (2013) 718–724.
[25] A. Tabet-Aoul, M. Mohamedi, Thin Solid Films 534 (2013) 270–274.
[26] Q. Xu, U. Linke, R. Bujak, T. Wandlowski, Electrochim. Acta 54 (2009) 5509–5521.
[27] S. Devan, V.R. Subramanian, R.E. White, J. Electrochem. Soc. 151 (2004) A905–A913.